

# Electrostatically Driven XY-stage Based on SOI-MEMS

Fuminori Bouno, Minoru Sasaki, and Kazuhiro Hane

Tohoku Univ., Dept. of Nanomechanics  
Aza-Aoba 01 Aramaki, Aoba-ku, Sendai 980-8579, Japan

## 1. Introduction

Technologies of probe microscope (e.g., SPM, SNOM) have been examined for increasing the density of the data storage. The recording bit size is required to decrease to nano scale (e.g., 25 nm for obtaining the density  $>1$  Tbit/in<sup>2</sup>). The millipede project is the exciting research in the group of IBM. For improving the throughput of the read/write time of SPM, thousands of probes are scanned in parallel. Each cantilever probe reads and writes in its own subfield. Usually, the pitch of the probe array is about 100  $\mu\text{m}$ . So, the media scanner is required to move  $>100\mu\text{m}$  in xy directions. MEMS actuator is expected to realize this task having the batch fabrication merit. The electrostatic actuator is preferred for decreasing the power consumption and the heat generation which can interfere the media performance.

In this study, xy-stage is fabricated based on Silicon-on-insulator (SOI) microelectromechanical systems (MEMS).

## 2. Device design

Figure 1 shows the schematic of xy two-dimensional actuator. The moving plate is at the center. For obtaining the larger x-axis displacement as a total, the actuator is designed to drive  $\pm$  directions. The comb pairs at left and right sides are for generating the half of the total displacement. The comb pairs are in three regions (indicated by three rightward arrows representing the force). One is at outer region (93.5 comb pairs). The others are two inner regions (25.5 comb pairs for each region). The fabricated suspensions have three different shapes (prebent, slant, and rectangular shapes). The schematic drawing of prebent and rectangular suspensions are shown in inset of Fig. 1. The slant spring has the straight beam having the slant angle. With the displacement, the suspension becomes nearly rectangle like the prebent one. The offset is 36  $\mu\text{m}$ . The difference compared to the design of Grade et al. is the offset direction of the paired suspensions. Since this actuator is designed to move  $\pm$  directions, the bending direction is opposite between suspensions at two (right and left) sides. The direction is set to become stable when the neighboring actuator works.

The driving along y-axis uses comb pairs at the center. Electrode pads for y-axis driving are at upside two corners in Fig. 1. The orthogonality between xy displacements is decided by the mask quality. The y-axis driving is designed at the resonance for obtaining the displacement amplification. The insulation between x- and y-axis electrodes is obtained using the epitaxially grown non-doped Si (width: 6  $\mu\text{m}$ ). The break down field for the non-doped crystal Si is 30 V/mm. The embedded epitaxial Si region is shown by black lines in Fig. 1.

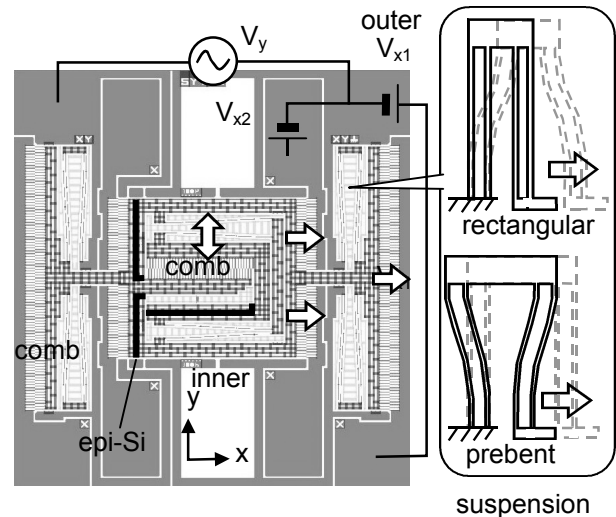


Fig.1: Schematic of xy two-dimensional actuator.

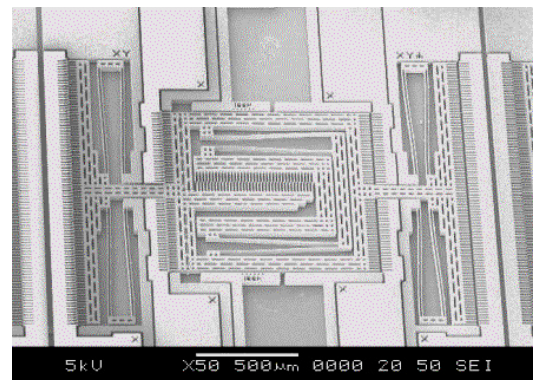


Fig.2: Fabricated two-dimensional actuator.

The comb drive actuator consists of two interdigitated finger structures. This device offers a nearly constant force coefficient against the driving voltage over large displacement, becoming a favorite electrostatic actuation scheme. Here, the limiting factor, which decides the maximum displacement, is the side instability, called "side snap-over". With the overlapping comb area, large cross-axis forces cause the sudden snap over sideways. The suspension that is compliant in one direction and stiff in the orthogonal directions is desired. Grade et al. introduced the design of prebent suspension as shown in the inset of Fig. 1 [2]. When the displacement occurs, the suspension becomes straight increasing the resistance to the side instability.

Figure 2 shows the actuator. The whole size is 2.4x2.3 mm including 8 electrodes. The device Si layer thickness is 50  $\mu\text{m}$ . The buried oxide thickness is 3  $\mu\text{m}$ . The fabrication is basically consists of two-time RIE etching. The 1st etching makes the trench, later filled with the epitaxial Si. The 2nd RIE decides the mechanical structure. By using the

vapor HF etching, the structure is released without the adhesion problem.

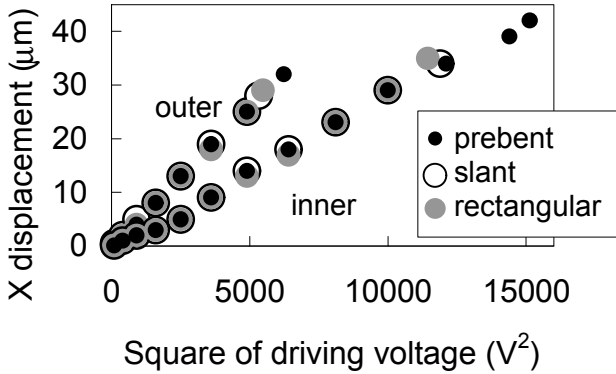


Fig.3: Obtained x-axis displacement.

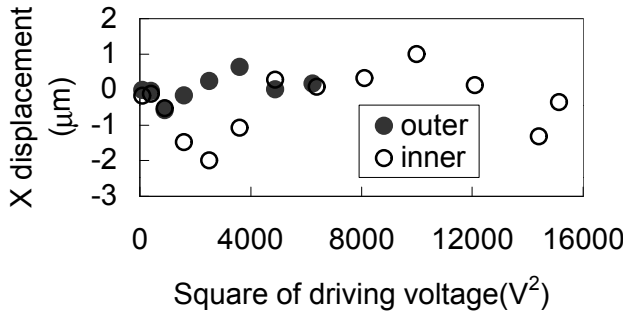


Fig.4: Difference from the linear relation.

### 3. Results

Figure 3 shows the x-axis displacement as a function of the square of driving voltage. The relation is in good agreement with the theoretical calculation. The linear the relation becomes, the more accurate the stage displacement control becomes. The displacement is measured until the instability occurs. The black filled, open, and gray circles correspond to suspensions having prebent, slant, and rectangular shapes, respectively. The prebent suspension gives larger displacement compared to the other. As for the instability parameter  $I$ , which is the ratio of the sideways electrostatic forces to the sideways suspension forces, this value is designed to be  $<1\%$  up to  $50\ \mu\text{m}$  displacement. This is lower than the measured value of  $20\text{-}50\%$  when the instability occurs in the reference [2]. Therefore, the instability occurs more easily compared to the estimation based on the case of reference. There are two data groups distributing on linear lines corresponding to the difference of the driving position (inner and outer regions for lower and upper groups, respectively). With the larger number of finger pairs, the outer electrode has the larger increasing ratio. The outer electrodes show the smaller maximum displacement although the driving voltage is lower. Since the generated force works far from the stage center, the unbalanced force can generate the larger moment which rotates the moving plate. The inner comb pair works more stably generating the larger displacement even at the higher driving voltage. The fact that the region of the inner comb pairs is geomet-

rically near to the center axis reduces the moment. Therefore, the total rigidity of moving plate against the unbalanced moment is the important factor.

The data is fitted by the straight line which passes the origin. The difference between them is shown in Fig. 4. The suspension is the prebent type. The comb finger is the standard rectangle in design. There is no overlap between comb fingers at the initial condition. S-shaped curve is obtained both for outer and inner region. The magnitude is  $\mu\text{m}$  level. The electrical field will not run between combs at the lower voltage. The displacement shows the relatively large value at the higher voltage. The electrical attraction working at the finger end surface will be the reason.

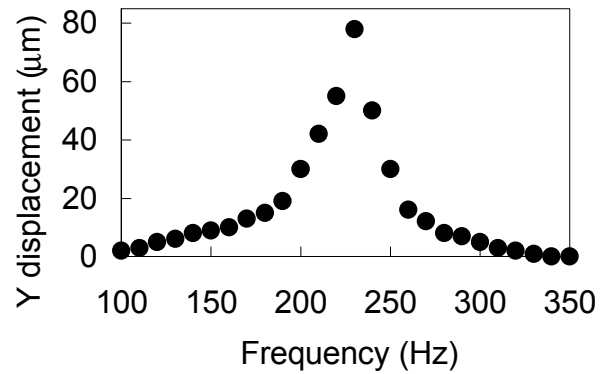


Fig.5: Obtained y-axis displacement.

Figure 5 shows the y-axis displacement as a function of the driving frequency.  $20\ \text{V}$  sinusoidal waves are applied. The resonant frequency is about  $230\ \text{Hz}$ . The displacement reaches  $80\ \mu\text{m}$  limited by the instability. This implies that the instability is mainly decided by the total mechanical rigidity, since the applied voltage is lower than the case of x-axis displacement. The layout (direction) of prebent suspension is same with that of x-axis one.

### 4. Conclusions

Electrostatically driven xy-stage is fabricated based on SOI-MEMS technique. The electrical isolation is obtained using the epitaxially grown Si. For x-axis driving, the whole displacement is divided into two (+ and -) directions.  $80\ \mu\text{m}$  displacement for both x- and y-axis is typically obtained. The displacement is near to the linear relation against the square of driving voltage, however the non-linearity exists. This will require the additional feedback control for the nm-level displacement control.

### Acknowledgements

The facilities used for this research include the Venture Business Laboratory at Tohoku University.

### References

- [1] P. Vettiger, G. Binnig, "The Nanodrive Project" Scientific American, Jan. pp. 47-53, 2003.
- [2] J. D. Grade, H. Jerman, T. W. Kenny, "Design of Large Deflection Electrostatic Actuators", J. MEMS, 12, pp. 335-343, 2003.